Computers and Geotechnics 36 (2009) 549–557

Contents lists available at ScienceDirect

Computers and Geotechnics

journal homepage: www.elsevier.com/locate/compgeo

Arbitrary Lagrangian–Eulerian method for dynamic analysis of geotechnical problems

M. Nazem [a,*], J.P. Carter [a], D.W. Airey [b]

[a] Centre for Geotechnical and Materials Modelling, The University of Newcastle, Callaghan, NSW 2308, Australia
[b] Centre for Geotechnical Research, The University of Sydney, NSW 2006, Australia

ARTICLE INFO

Article history:
Received 30 June 2008
Received in revised form 28 October 2008
Accepted 5 November 2008
Available online 12 December 2008

Keywords:
ALE method
Time-stepping
Viscous boundaries
Dynamic analysis

ABSTRACT

In this paper an arbitrary Lagrangian–Eulerian (ALE) method to solve dynamic problems involving large deformation is presented. This ALE method is based upon the operator-split technique in which the material displacements and mesh displacements are uncoupled. A brief history of the ALE method is first presented and then special issues such as time-stepping, mesh refinement, energy absorbing boundaries, dynamic equilibrium checks and remapping of state variables are explained. The ALE method and the updated-lagrangian (UL) method are then used to analyse some geotechnical problems to examine the significance of inertia effects, large deformation and contact mechanics. The results show the efficiency of the ALE method for solving dynamic geotechnical problems involving large deformation.

1. Introduction

In many geotechnical problems, it is vital to consider the geometrical nonlinearity caused by large deformation in order to capture more realistic behaviour. The solutions so obtained should then be more accurate and reliable, which should ultimately lead to cheaper and safer design. For example, highway embankments built on very soft clay deposits can undergo settlements in the order of 1–10 m without undergoing a conventional bearing capacity failure. Such large movements warrant a large deformation approach in the analysis of the embankment behaviour. Another example is the installation of displacement piles, which are essential components of the foundations of many offshore platforms. During installation, significant changes of geometry occur that should not be neglected in an analysis of the effects of pile installation on the surrounding soil. There is also a wide range of geotechnical problems where dynamic loads are applied to soil in which the effects of inertia forces should not be ignored. For example, in problems such as dynamic compaction and rapid penetration of objects into soil, the propagation of stress waves through the ground may involve large stress and strain amplitudes. These problems also involve large deformations. One possible and robust way to solve dynamic problems involving large deformations is to take advantage of the arbitrary Lagrangian–Eulerian (ALE) method.

The ALE method was first developed in fluid mechanics for modelling the motion of free surfaces and boundary conditions. The concept of ALE was initially suggested by Noh [20] under the term 'coupled Eulerian–Lagrangian', where the method was implemented in a finite difference framework to solve two-dimensional hydrodynamics problems with moving fluid boundaries. Later, the method was extended to two-dimensional and three-dimensional flow problems, respectively, by Hirt et al. [7] and Stein et al. [25]. One of the first implementations of the ALE method into the finite element framework was performed by Belytschko and Kennedy [2] in response to the need for nonlinear simulation techniques in nuclear safety analyses in which fluid–structure interaction problems are usually confronted. The main advantage of the ALE method in fluid–structure interaction problems is that the fluid can be handled by the ALE formulation while the structure is analysed by a Lagrangian method. Belytschko and Kennedy [2] considered inviscid compressible fluids in their proposed ALE approach, while Hughes et al. [11] presented a finite element procedure for viscous incompressible flows and free surface flows in conjunction with a general kinematical theory for the ALE method.

As indicated above, the ALE method originated from the field of fluid mechanics. However, researchers realised that the method could be applied to problems in solid mechanics involving large deformations. The main drawbacks of the Lagrangian methods are known to be mesh distortion and entanglement of finite elements in problems with relatively large deformations. But, mesh distortion can be prevented by decoupling the mesh displacements and the material displacements, which is the basic idea underlying the ALE method. The separation of material displacements and mesh displacements introduces two sets of unknowns in the global equations. The ALE strategy is called 'coupled' if all unknown

* Corresponding author. Tel.: +61 249216048; fax: +61 249216991.
E-mail address: majidreza.nazem@newcastle.edu.au (M. Nazem).

0266-352X/$ - see front matter © 2008 Elsevier Ltd. All rights reserved.
doi:10.1016/j.compgeo.2008.11.001

equations are solved simultaneously for material displacements as well as mesh displacements, otherwise it is referred to as 'decoupled' or the operator-split technique. In a coupled ALE procedure some additional equations are required to solve the governing system of equations. These extra equations provide relations between the material points and mesh points and are usually referred to as supplementary equations. Moreover, since the material points do not coincide with the mesh points, all path-dependent state variables such as stresses need to be mapped from the material points to the mesh points. Hughes et al. [11] suggested a first order expansion of Taylor's series for remapping the stresses, which is also known as the convection equation

$$\dot{\sigma}^r = \dot{\sigma} + (v_i - v_i^r) \cdot \frac{\partial \sigma}{\partial x_i} \tag{1}$$

where $\dot{\sigma}^r$ and $\dot{\sigma}$ denote the time derivatives of stresses with respect to the mesh and material coordinates, respectively, v_i is the material velocity, and v_i^r represents the mesh velocity.

One of the earliest applications of the ALE method in solid mechanics was performed by Liu et al. [15], in which path-dependent materials were considered. Liu et al. [15] derived the conservation equations in the ALE coupled framework and introduced stress-velocity products to avoid computing the spatial derivatives of stress in the convection equation. Later, Liu et al. [16] generalised the same formulation for the Petrov–Galerkin finite element procedure. In both studies the governing equations were solved in a coupled form with an implicit time-integration scheme, and an automatic mesh generator based upon the Laplace equation was used to supply the supplementary equations.

Benson [3] proposed the ALE operator-split technique to decouple mesh displacements and material displacements. To solve the equilibrium equations by this technique, two steps are considered in the analysis: an updated-lagrangian (UL) step followed by an Eulerian step. In the UL step, the convection terms are neglected and the UL method is used to solve the equilibrium equation. In the Euler step, a new mesh is generated for the deformed domain and all state variables are then transferred from the old mesh to the new mesh. By using the operator-split technique, Benson [3] found that the cost of large deformation analysis could be reduced by a factor of two without a significant loss in accuracy.

Some improvements to the ALE method were obtained by applying the approach to different problems of solid mechanics. Huetink and Vreede [9] extended the operator-split technique with an explicit time integration to contact problems and simulated the "upsetting" process in metals forming. Ghosh and Kikuchi [6] presented an ALE coupled formulation for elasto-viscoplastic materials and solved various problems in metals forming. Yamada and Kikuchi [26] presented an ALE coupled formulation in terms of total deformation for incompressible hyperelastic materials.

An overall description of the ALE method was presented by Huerta and Casadei [10] where the main challenge addressed was its extension to problems of solid mechanics including path-dependent materials such as soils. It was suggested that the major difficulties in an ALE implementation are the mesh optimisation scheme and a low-cost algorithm for convecting state variables. However, no practical scheme was presented by the authors. Gadala and Wang [5] derived the governing equations of the ALE method in a coupled form with both the Jaumann and Truesdell stress rates. The main contribution of this work was assuming a linear function between the mesh displacements and the material displacements which then allows for setting up the supplementary equations at the element level instead of at the global level. Although this procedure required modifying the element stiffness matrices, the number of equations to be solved remained the same as in a Lagrangian formulation. The supplementary equations at the element level were then obtained by a mesh generator algorithm based on a transfinite mapping technique which could maintain a homogeneous mesh throughout the analysis.

Rodriguez-Ferran et al. [21] presented an ALE formulation for hyper-elastoplastic materials based upon the operator-split technique. The new idea in this formulation, in contrast to previous ALE formulations for hyper-elastoplasticity, was choosing the deformed configuration at the beginning of the time-step as the ALE reference configuration instead of the initial undeformed configuration. Consequently, only the elastic component of strains must be remapped from the distorted mesh to the new mesh during the convection phase. It should be noted that if the initial undeformed configuration is chosen as the ALE reference domain, the plastic part of strains must also be transported during the convection step. Solution to three different problems including a necking test, a coining test and a powder compaction test were obtained by this method and the results were compared with those obtained using the UL method. This comparison clearly showed that it is very important to avoid mesh distortion during an ALE analysis since the quality of numerical solutions can be affected.

Bayoumi and Gadala [1] presented a complete derivation and implementation of the coupled ALE formulation for both static and dynamic analysis of large deformation problems. This research also presented a new method for remapping the stresses from the old mesh to the new mesh which did not require the computation of stress gradients. The formulation was then implemented into a $2D$ finite element code and several example problems, including those involving elastoplastic materials, were solved.

Recently, the ALE method has attracted attention in solving geotechnical problems. Hu and Randolph [8] proposed a numerical procedure for large deformation problems in soils which, in their opinion, falls within the ALE category. They combined the conventional small strain finite element method with an automatic mesh generation algorithm and a linear stress interpolation technique to deal with plane strain and axisymmetric problems such as cavity expansion and the bearing capacity of footings. They found this technique to be a practical approach which could make the most use of a small strain finite element code and yet still provide accurate solutions for problems that involve large-strains and deformations. Nazem et al. [18] presented a new mesh optimisation technique to be used with the operator-split technique for solving large deformation problems in geomechanics. Later, Nazem et al. [19] presented an ALE formulation for solving consolidation problems in geomechanics. They showed the efficiency and robustness of the ALE method by solving some classical problems such as consolidation of footings and cavity expansion.

The application of the ALE method in dynamic analysis of geotechnical problems and its complexity are the subject of this paper. An ALE method based on the operator-split technique for solving dynamic geotechnical problems is presented and its key aspects are explained. The performance and capability of the method are demonstrated by analysing a rigid footing under statically, as well as dynamically, applied vertical pressure, and the rapid indentation of a rigid cylinder into a layer of soil. The effect of rapid loading on the behaviour of these problems is also demonstrated by performing several small deformation and large deformation analyses.

2. Finite element formulation

2.1. Momentum equation

In the updated-lagrangian (UL) method, we assume that the analysis starts at time 0 and all state variables that satisfy dynamic equilibrium are known up to time t. Further loading and deformation of the body will require the dynamic equilibrium to be satisfied at time $t + \Delta t$. The equation of motion is given by

$$\mathbf{M}\ddot{\mathbf{u}}^{t+\Delta t} + \mathbf{C}\dot{\mathbf{u}}^{t+\Delta t} + \mathbf{F}_{int}^{t+\Delta t} = \mathbf{F}_{ext}^{t+\Delta t} \tag{2}$$

where $\mathbf{M}$ and $\mathbf{C}$ are the mass and damping matrices, respectively, $\mathbf{u}$ represents the displacement vector, $\mathbf{F}_{int}$ is the internal force vector and $\mathbf{F}_{ext}$ denotes the external force vector. The right superscript denotes the time when the quantities are measured and a superimposed dot represents the time derivative of a variable.

2.2. Time integration

To solve the momentum equation in (2), a step-by-step integration scheme must be employed to obtain the solution in the time domain. There are several time-integration algorithms commonly used in geotechnical problems. Recently, Kontoe et al. [13] studied the performance of such algorithms for geotechnical problems and observed that the generalised-α method presented by Chung and Hulbert [4] has qualities superior to those of the other algorithms investigated. The generalised-α method was developed to obtain second-order accuracy, minimal numerical dissipation of lower modes and maximum numerical dissipation of higher modes in structural dynamics. This particular method of time integration is adopted in this study.

In the generalised-α method, the displacements and velocities are computed using equations similar to those in Newmark's method, i.e.,

$$\begin{aligned}\mathbf{u}^{t+\Delta t} &= \mathbf{u}^{t} + \dot{\mathbf{u}}^{t}\cdot\Delta t + \left[\left(\frac{1}{2}-\beta\right)\cdot\ddot{\mathbf{u}}^{t} + \beta\cdot\ddot{\mathbf{u}}^{t+\Delta t}\right]\cdot\Delta t^2\\ \dot{\mathbf{u}}^{t+\Delta t} &= \dot{\mathbf{u}}^{t} + [(1-\delta)\cdot\ddot{\mathbf{u}}^{t} + \delta\cdot\ddot{\mathbf{u}}^{t+\Delta t}]\cdot\Delta t\end{aligned} \tag{3}$$

where β and δ are the Newmark integration parameters and Δt represents the time-step. In the method of Chung and Hulbert [4] which is also adopted here, two new integration parameters, α_f and α_m, are introduced into the momentum equation to compute the inertia forces at time $t+(1-\alpha_m)\Delta t$ and the internal and damping forces at time $t+(1-\alpha_f)\Delta t$, respectively. Therefore, the momentum equation can be written as follows:

$$\begin{aligned}&\mathbf{M}[(1-\alpha_m)\cdot\ddot{\mathbf{u}}^{t+\Delta t} + \alpha_m\cdot\ddot{\mathbf{u}}^{t}] + \mathbf{C}[(1-\alpha_f)\cdot\dot{\mathbf{u}}^{t+\Delta t} + \alpha_f\cdot\dot{\mathbf{u}}^{t}]\\ &\quad + (1-\alpha_f)\cdot\mathbf{F}_{int}^{t+\Delta t} + \alpha_f\cdot\mathbf{F}_{int}^{t} = (1-\alpha_f)\cdot\mathbf{F}_{ext}^{t+\Delta t} + \alpha_f\cdot\mathbf{F}_{ext}^{t}\end{aligned} \tag{4}$$

The nonlinear equation in (4) can be solved by an iterative scheme. If we employ the Newton–Raphson method, the following equations must be solved during the ith iteration:

$$\begin{aligned}&\left[\frac{1-\alpha_m}{\beta\cdot\Delta t^2}\cdot\mathbf{M} + \frac{\delta(1-\alpha_f)}{\beta\cdot\Delta t}\cdot\mathbf{C} + (1-\alpha_f)\cdot\mathbf{K}_{(i-1)}\right]\cdot\Delta\mathbf{u}_{(i)}\\ &\quad = (1-\alpha_f)\cdot\mathbf{F}_{ext}^{t+\Delta t} + \alpha_f\cdot\mathbf{F}_{ext}^{t} - (1-\alpha_f)\cdot\mathbf{F}_{int(i-1)}^{t+\Delta t} - \alpha_f\cdot\mathbf{K}_{(i-1)}\cdot\mathbf{u}^{t}\\ &\qquad - \mathbf{M}\left[\frac{1-\alpha_m}{\beta\cdot\Delta t^2}\cdot(\mathbf{u}_{(i-1)}^{t+\Delta t} - \mathbf{u}^{t}) - \frac{1-\alpha_m}{\beta\cdot\Delta t}\cdot\dot{\mathbf{u}}^{t} - \left(\frac{1-\alpha_m}{2\beta}-1\right)\cdot\ddot{\mathbf{u}}^{t}\right]\\ &\qquad - \mathbf{C}\left[\frac{\delta(1-\alpha_f)}{\beta\cdot\Delta t}\cdot(\mathbf{u}_{(i-1)}^{t+\Delta t} - \mathbf{u}^{t}) + \left(1-\frac{\delta}{\beta}(1-\alpha_f)\right)\cdot\dot{\mathbf{u}}^{t}\right.\\ &\qquad \left. -\Delta t\left(\frac{\delta}{2\beta}-1\right)(1-\alpha_f)\cdot\ddot{\mathbf{u}}^{t}\right]\mathbf{u}_{(i)}^{t+\Delta t} = \mathbf{u}_{(i-1)}^{t+\Delta t} + \Delta\mathbf{u}_{(i)}, \quad \mathbf{u}_{(0)}^{t+\Delta t} = \mathbf{u}^{t}\end{aligned} \tag{5}$$

in which $\mathbf{K}$ is the tangent stiffness matrix and $\mathbf{F}_{int}$ is obtained by

$$\mathbf{F}_{int}^{t+\Delta t} = \int_{V^{t+\Delta t}} \mathbf{B}^{T}\cdot\boldsymbol{\sigma}^{t+\Delta t}dV^{t+\Delta t} \tag{6}$$

where $\boldsymbol{\sigma}$ represents the true (Cauchy) stress vector, $\mathbf{B}$ is the linear strain-displacement transformation matrix and V denotes the volume of an element.

2.3. Stress integration

In each time-step of a nonlinear finite element analysis, a set of equations must be solved to find the stress increment based upon the known strain increment. This system of equations may be written as

$$\dot{\sigma}_{ij} = C_{ijkl}^{ep}\cdot\dot{\varepsilon}_{kl}, \quad \dot{\kappa}_i = B_i(\sigma,\kappa)\cdot\dot{\lambda} \tag{7}$$

where ε denotes the strain tensor, κ represents a set of hardening parameters, B is a function derived from the hardening laws, and

$$C_{ijkl}^{ep} = C_{ijkl}^{e} - \frac{C_{ijmn}^{e}\cdot\frac{\partial f}{\partial\sigma_{mn}}\cdot C_{klpq}^{e}\cdot\frac{\partial g}{\partial\sigma_{pq}}}{\frac{\partial f}{\partial\sigma_{pq}}\cdot C_{pqrs}^{e}\cdot\frac{\partial f}{\partial\sigma_{rs}} - \frac{\partial f}{\partial\kappa_m}\cdot B_m(\sigma,\kappa)} \tag{8}$$

$$\dot{\lambda} = \frac{\frac{\partial f}{\partial\sigma_{ij}}\cdot C_{ijkl}^{e}\cdot\dot{\varepsilon}_{kl}}{\frac{\partial f}{\partial\sigma_{ij}}\cdot C_{ijkl}^{e}\cdot\frac{\partial g}{\partial\sigma_{kl}} - \frac{\partial f}{\partial\kappa_m}\cdot B_m(\sigma,\kappa)} = D_{kl}\cdot\dot{\varepsilon}_{kl} \tag{9}$$

in which C^e represents the elastic stress–strain matrix, f is a yield surface describing the elastic domain, g is the plastic potential function, and $\dot{\lambda}$ is a positive scalar called the plastic multiplier. For large deformation analysis, the stress–strain relations can no longer be expressed by Eq. (7) since the components of the true stress change due to possible rigid body motion. In other words, the principle of objectivity requires that a stress–strain relation must be independent of the observer, i.e., rigid body rotation must induce no extra strain in the material. Objectivity is usually satisfied by introducing a frame-independent stress rate into the stress–strain relations. The choice of the objective stress rate is not unique and the most commonly used stress rates are the Jaumann stress rate and the Truesdell stress rate (e.g., see Nazem et al. [18]). Introducing, for instance, the Jaumann stress rate into the constitutive equations, one can write

$$\begin{aligned}\sigma_{ij}^{t+\Delta t} &= \sigma_{ij}^{t} + \int_0^{\Delta\varepsilon_{ij}} \mathrm{d}\sigma_{ij}\\ &= \sigma_{ij}^{t} + \int_0^{\Delta\omega_{kl}} (\sigma_{ik}\cdot\mathrm{d}\omega_{jk} + \sigma_{jk}\cdot\mathrm{d}\omega_{ik}) + \int_0^{\Delta\varepsilon_{kl}} C_{ijkl}(\sigma,\kappa)\cdot\mathrm{d}\varepsilon_{kl}\end{aligned} \tag{10}$$

where ω is the spin tensor. In this study, an explicit scheme based on the work by Sloan et al. [23,24] is used to perform the integrations in Eq. (10). This scheme was originally developed for stress-integration in a small strain analysis and then it was generalised for large deformation problems by Nazem et al. [18].

2.4. Energy absorbing boundaries

One of the well-known issues in computational dynamic analysis of soil-structure-interaction (SSI) problems is how to simulate an infinite medium. Employing the finite element method, for instance, with boundaries that are not infinitely distant, one must guarantee that the outgoing waves from the source (usually a structure) do not reflect back from the finite boundaries toward the source, since in reality these waves should propagate to infinity and dissipate at a far distance from the source. If it is allowed to occur, such reflection will most probably affect the accuracy of the numerical results. To assure no waves are reflected back from truncated computational boundaries, it is common to use artificial boundaries which absorb the energy of incoming waves. A simple, but efficient, boundary was developed by Lysmer and Kuhlemeyer [17] which is known as the "standard viscous boundary" in the literature. The standard viscous boundary is probably the most popular artificial boundary since it possesses an acceptable dissipation characteristic at a low computational cost. Kellezi [12] suggests that absorbing boundaries must not be located closer than $(1.2–1.5)\lambda_s$ (where λ_s is the length of the shear waves) from the

excitation source. A recent study by Kontoe [14] showed that the standard viscous boundary is capable of absorbing dilatational waves (P-waves) as well as shear waves (S-waves) in the analysis of plane strain and axisymmetric SSI problems. When required, this type of boundary was used in the problems solved in this study. It is briefly explained in the following.

To implement the standard viscous boundaries into a finite element code, one must consider the momentum equation in (2) for each individual element and replace the element damping matrix $\mathbf{C}$ by

$$\bar{\mathbf{C}} = \mathbf{C} + \mathbf{C}_B \tag{11}$$

where $\bar{\mathbf{C}}$ represents the new element damping matrix, and $\mathbf{C}_B$ is the contribution from the standard viscous boundary given by

$$\mathbf{C}_B = \int_L \mathbf{N}^T \mathbf{C}_c \mathbf{N} \mathrm{d}L \tag{12}$$

in which L is the side of the element being modelled as the viscous boundary, $\mathbf{N}$ contains the element shape functions on L, and $\mathbf{C}_c$ is the constitutive viscous damping matrix depending on the material properties of the element. This matrix for plane strain and axisymmetric conditions is computed according to

$$\mathbf{C}_c = \rho \begin{bmatrix} V_s & 0 \\ 0 & V_p \end{bmatrix} \tag{13}$$

where ρ is the mass density, and V_p and V_s represent, respectively, the velocity of dilatational waves and shear waves which for an elastic medium are defined by

$$V_s = \sqrt{\frac{E}{2\rho(1+\nu)}} \tag{14}$$

$$V_p = \sqrt{\frac{E(1-\nu)}{\rho(1+\nu)(1-2\nu)}} \tag{15}$$

in which E is the Young's modulus and ν is the Poisson's ratio.

3. Arbitrary Lagrangian–Eulerian method

3.1. Operator-split technique

The most significant drawback of the UL method is mesh distortion and entanglement of the elements in problems involving relatively large deformations. The ALE method has been developed based on the idea of separating the material and mesh displacements to eliminate mesh distortion in the UL method. This separation introduces unknown mesh displacements into the governing global system of equations, in addition to the unknown material displacements. In the so-called coupled ALE method, a supplementary set of equations in terms of the material and mesh displacements is established through a mesh motion scheme and the two sets of unknown displacements are then solved simultaneously.

On the other hand, the decoupled ALE method, or the operator-split technique, first solves the material displacements via the momentum equation and then computes the mesh displacements through a mesh refinement technique. In this method, the analysis is performed in two steps: an UL step followed by an Eulerian step. In the UL step, we solve the governing equations to fulfil equilibrium and obtain the material displacements. In the Eulerian step, a new mesh is generated for the deformed domain to obtain the mesh displacements. All dynamic and static variables are then transferred from the distorted mesh to the new mesh. The key issues in the operator-split ALE method thus include the mesh optimisation in the Euler step and the mapping of variables between the two meshes.

To obtain the mesh displacements, we first re-discretise the deformed boundaries resulting from the UL step. These boundaries include the boundaries of the domain, the material interfaces and the loading boundaries. With known displacements of the nodes on these boundaries, we then perform an elastic static analysis using prescribed displacements to obtain the optimal mesh and hence the mesh displacements for all the internal nodes. An important advantage of this mesh optimisation method is its independence of element topology and problem dimensions. The method does not require any mesh generation algorithm, does not change the topology of the problem, and hence can be easily implemented in existing finite element codes. For more details see Nazem et al. [18].

3.2. Remapping of state variables

The remapping of state variables from the old (material) mesh to the new (grid) mesh during an ALE analysis is very important. Generally speaking, two sets of variables must be considered for remapping; variables at integration (Gauss) points such as components of stress and hardening parameters and those at nodal points such as displacements, velocities and accelerations. In each case, remapping is usually performed using a first order expansion of Taylor's series

$$\dot{f}^r = \dot{f} + (v_i - v_i^r) \cdot \frac{\partial f}{\partial x_i} \tag{16}$$

where $\dot{f}^r$ and $\dot{f}$ denote the time derivatives of an arbitrary function f with respect to the mesh and material coordinates, respectively. The procedure for remapping variables at integration points is given in a recent paper (see [18]). Here, we briefly explain a simple, but efficient, procedure for remapping nodal velocities and nodal accelerations. Multiplying Eq. (16) by the time increment and substituting the acceleration for function f gives (the same procedure is used for remapping nodal velocities)

$$\ddot{u}^r = \ddot{u} + (u_i - u_i^r) \cdot \frac{\partial \ddot{u}}{\partial x_i} \tag{17}$$

Eq. (17) is applied on each node per element to compute the new nodal accelerations. To find the gradients of acceleration, we take advantage of the normal coordinates ξ and η as follows:

$$\frac{\partial \ddot{u}}{\partial x_i} = \frac{\partial \ddot{u}}{\partial \xi} \cdot \frac{\partial \xi}{\partial x_i} + \frac{\partial \ddot{u}}{\partial \eta} \cdot \frac{\partial \eta}{\partial x_i} \tag{18}$$

in which the derivatives of the acceleration with respect to the normal coordinates can be obtained using the displacement shape functions N_i

$$\frac{\partial \ddot{u}}{\partial \xi} = \sum_{i=1}^{n} \frac{\partial N_i}{\partial \xi} \cdot \ddot{u}^i, \quad \frac{\partial \ddot{u}}{\partial \eta} = \sum_{i=1}^{n} \frac{\partial N_i}{\partial \eta} \cdot \ddot{u}^i \tag{19}$$

where n represents the number of nodes per element and $\ddot{u}^r$ represents the nodal accelerations.

The transformation of state parameters between the old mesh and the new mesh does not guarantee that dynamic equilibrium and the local consistency conditions are satisfied. To the authors' knowledge, there is no simple solution to this problem available in the literature to date. Therefore, dynamic equilibrium and the local consistency must be checked again. To bring the system to equilibrium, additional Newton–Raphson iterations may be needed, and test runs indicate that typically 2–5 iterations are required to satisfy the momentum equation to sufficient accuracy.

4. Numerical example

The ALE method for dynamic analysis of problems involving large deformations was explained in the previous sections. This method has been implemented into the finite element code, SNAC, developed at the University of Newcastle, Australia. This code is used for all the numerical examples presented in this section. Although the ALE method can be utilised in dynamic analysis of general types of large deformation problems in solid mechanics, we limit our applications here to small strain cavity expansion under impulse loading, and large deformation problems that involve mobilisation of the dynamic bearing capacity of a footing on a Tresca material and the rapid indentation of a cylinder into a layer of elastoplastic soil.

4.1. Expansion of spherical cavity under internal impact pressure

The response of a spherical cavity in an infinite elastic medium to an impulse loading is one of the few problems of its type for which an analytical solution exists in the literature [22]. This problem is examined here to verify the dynamic finite element formulation and its implementation. The problem, material properties and the boundary conditions are depicted in Fig. 1. E, ν, P_0 and R in Fig. 1 represent the Young's modulus and Poisson's ratio of the elastic soil, the internal pressure and the radius of the cavity, respectively. Unit mass density, ρ, is assumed for the soil. In the finite element analysis an internal pressure of overall intensity P_0 was applied to the cavity boundary over 20 equal time increments covering a period of 0.01 s, i.e., as a steeply ramped impulse loading. This pressure was then held constant during the remainder of the analysis. The dynamic analysis was continued for a total period of 0.25 s. The UL method and the ALE method were used to obtain a solution. Since no serious mesh distortion occurs, the UL and ALE methods provided identical results in this example.

Fig. 2 shows the relation between the radial displacement of a point on the internal boundary versus time, obtained from the analytical solution for an instantaneously applied cavity pressure, as well as by the finite element method assuming steeply ramped pressure. There is a good agreement between the two solutions which validates the finite element formulation for dynamic problems presented here. It can be observed from these solutions that the inertial effects in the elastic medium result in a transient increase (or "overshoot") in the radial displacement of the cavity boundary. As time progresses this displacement reduces to its steady state value. The magnitude of the overshoot is significant, being about 30% of the final steady state displacement.

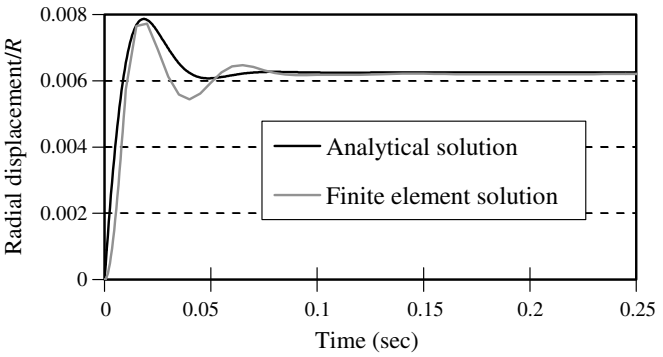

Fig. 2. Radial displacement versus time.

4.2. Footing on undrained soil

In this example, a rough rigid footing loading an undrained soil layer is considered. The mesh for the right-hand half of the footing and the material properties are shown in Fig. 3. Note that E, c_u and ν in Fig. 3 represent the Young's modulus, undrained shear strength and Poisson's ratio of the soil, respectively. Zero undrained friction angle and unit mass density, ρ, were assumed for the soil. Poisson's ratio is considered to be 0.49 in order to take into account the elastic incompressibility of the material under undrained conditions. Similarly, an associated Tresca model is used to represent the plastic incompressibility of the purely cohesive soil deforming under such conditions. The mesh consists of 872 6-noded plane-strain triangular elements, with 1817 nodes overall.

The footing was first analysed assuming small deformation only. A pressure-defined static load was applied to the footing and the analysis stopped due to lack of convergence as the pressure reached $5.4c_u$. This value represents the numerically predicted collapse load of the footing, which is about 5% above the Prandtl solution obtained from plasticity theory, i.e., $(2+\pi)c_u \approx 5.14c_u$.

The footing was then reanalysed using a dynamic small strain approach. In one case the loading was applied rapidly, at a rate of $20.0c_u$/s, so that theoretically a total pressure of $20c_u$ would be applied over a period of 1 s, while in the other the rate of loading was slower at $2.0c_u$/s, corresponding to a total pressure of $20c_u$ being applied in 10 s. In both cases, inertia forces were taken into account and no viscous damping was assumed. The load–displacement curves for these analyses are shown in Fig. 4a. The collapse loads of the footing for rapid and slower loading were predicted to be $12.3c_u$ and $6.6c_u$, respectively. These values are 120% and 22% above the collapse load obtained by the static analysis.

The problem was then solved in a similar fashion with identical load rates but assuming large deformations. Both static and dynamic analyses were performed. The load–displacement curves for the large deformation analyses are shown in Fig. 4b. In the static analysis and the dynamic analysis with slow loading a lack of convergence of the solution was observed (i.e., equilibrium was not satisfied) at applied pressures of $6.25c_u$ and $8.52c_u$, respectively. This lack of convergence should not necessarily be taken as an indication of reaching the ultimate load in these cases. It is to be expected that the ultimate load would only be mobilised

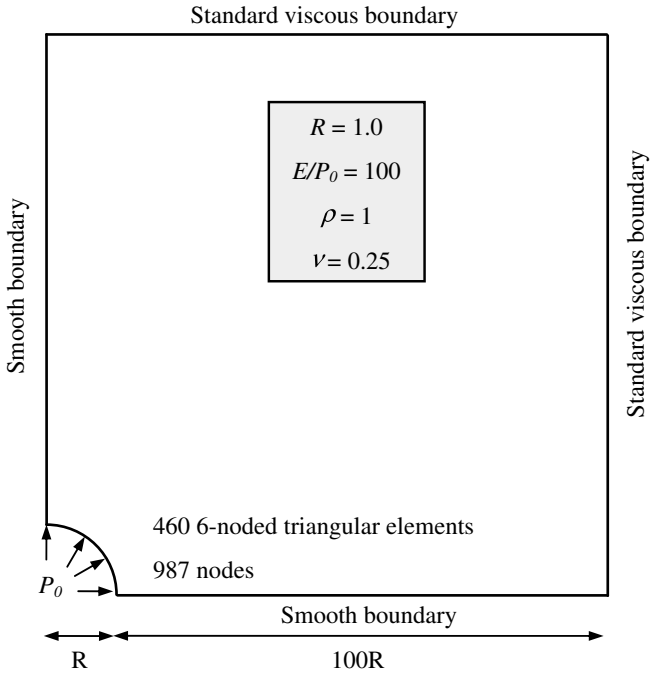

Fig. 1. Rigid rough footing on cohesive soil.

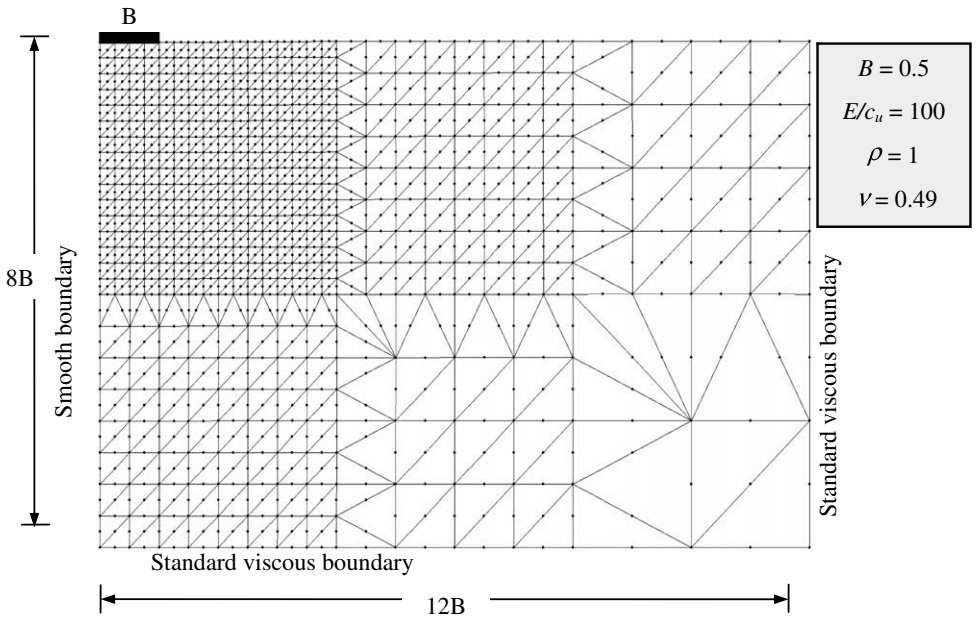

Fig. 3. Rigid rough footing on cohesive soil.

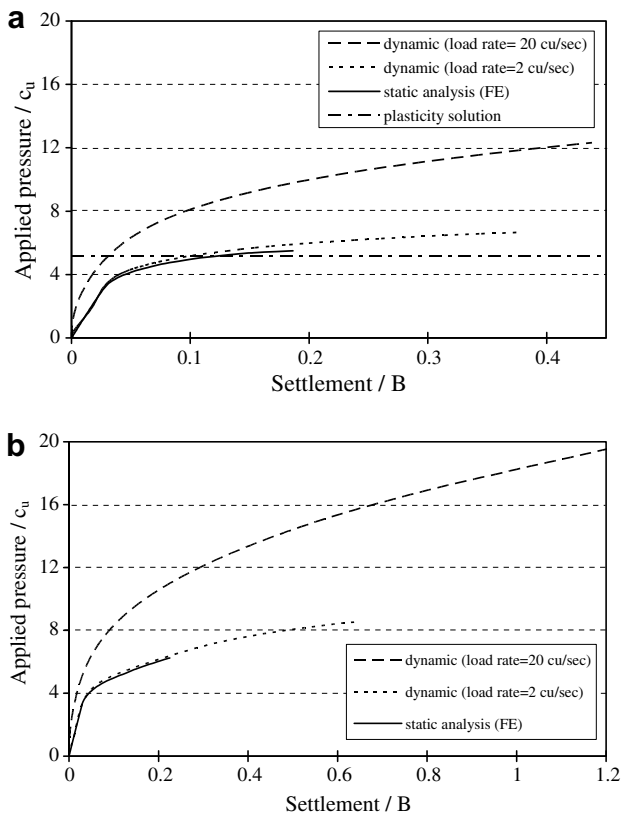

Fig. 4. Load–displacement curves. (a) Small deformation analysis; and (b) large deformation analysis (ALE method).

when the footing becomes deeply buried within the soil layer (deeper than explored in the current analysis). Nevertheless, it is noted that these values of applied pressure at the point of non-convergence are 21% and 66% larger than the Prandtl solution obtained from the theory of plasticity assuming small deformations. Similarly, a clearly identifiable collapse load was not identified in the rapid loading analysis.

It is important to emphasise that the higher footing stiffness predicted by the dynamic analyses, in both the small and large deformation cases reported here, result from inertia effects alone. Material rate effects have not been considered in these analyses.

It is also worth noting that the large deformation results presented in Fig. 4b were all obtained by the ALE method. For the static analysis and the dynamic analysis involving slow loading, the results obtained by the UL method coincide with the ALE predictions, since no severe mesh distortion occurs during the analysis. However, the UL method could not simulate the dynamic response under rapid loading due to the severe mesh distortion that occurred at a loading time of approximately 0.9 s. This distorted mesh is shown in Fig. 5a. The deformed mesh obtained by the ALE method at the end of the rapid loading analysis is shown in Fig. 5b. No unacceptable mesh distortion can be observed in the latter case.

4.3. Dynamic indentation of a cylinder into a soil layer

In this example, we study the indentation of a long rigid cylinder into an undrained layer of soil. To simulate undrained conditions, the soil is modelled by an associated Tresca material. Due to symmetry, only the right-hand half of the problem is considered, as shown in Fig. 6. The diameter of the cylinder is assumed to be D and the material properties are the same as those in example 4.2. The mesh consists of 1392 4-noded plane-strain rectangular elements and 1465 nodes. The problem involves large deformations as well as contact mechanics. The coefficient of friction between the cylinder and the soil is assumed to be 0.01. A static analysis as well as a dynamic analysis were performed to simulate the indentation of the cylinder and to examine the significance of the inertia forces. In the static analysis, a total indentation of $2D$ was applied. For the dynamic analysis, the indentation was prescribed at a constant velocity of $2D$ per second.

The UL method was unable to finish the numerical analysis due to severe mesh distortion. By contrast, the ALE method could complete the analysis to the prescribed indentation. Fig. 7 shows plots of indentation normalised by the diameter of the cylinder, D, versus the applied force per unit length normalised by the product of the diameter, D, and the undrained shear strength, c_u, obtained

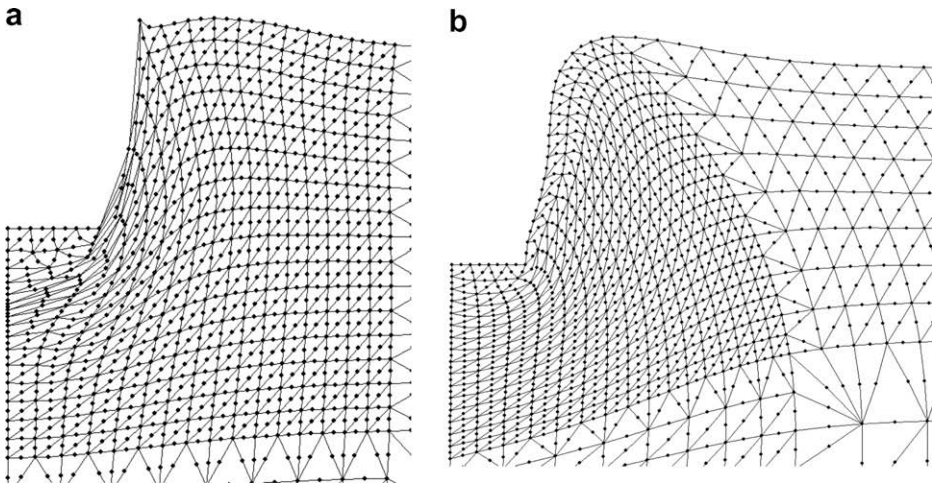

Fig. 5. Deformed meshes for the case of rapid loading. (a) UL method, $t = 0.9$ s; and (b) ALE method, $t = 1.0$ s.

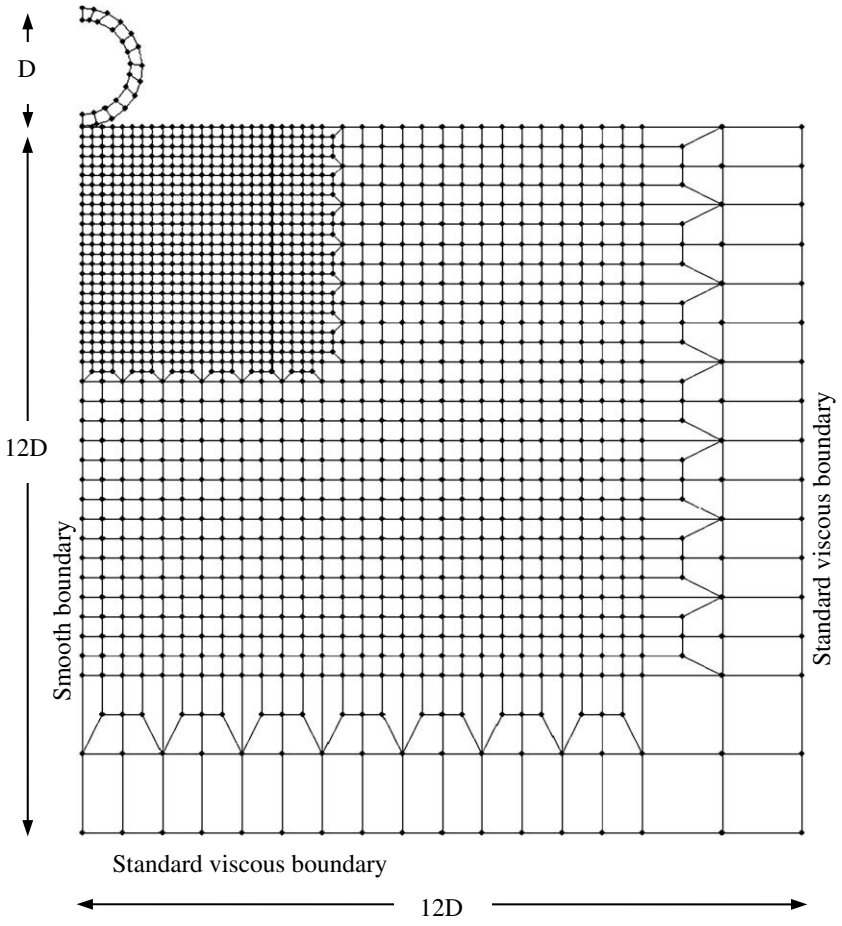

Fig. 6. Rigid cylinder on cohesive soil.

by the ALE method under static as well as dynamic loading. According to these plots, no obvious failure load was observed within the limits of this analysis, i.e., for indentations up to 2*D*. It is expected that a limiting load would be reached if the indentation was continued and the cylinder became buried more deeply in the soil. However, even at the relatively shallow indentations considered here, an increase in soil resistance can be observed due to the presence of inertia forces in the dynamic analysis. Fig. 8 represents this increase in soil resistance plotted against the indentation. The effect of numerical overshoots in the dynamic response has been overlooked in this plot. The plotted increase is significant for indentations less than approximately 1.5*D*. The static and dynamic responses are similar for indentations larger than 1.5*D*.

To represent the capability of the ALE method, the deformed mesh at the end of dynamic analysis is shown in Fig. 9. No severe mesh distortion can be observed in the final mesh. This example

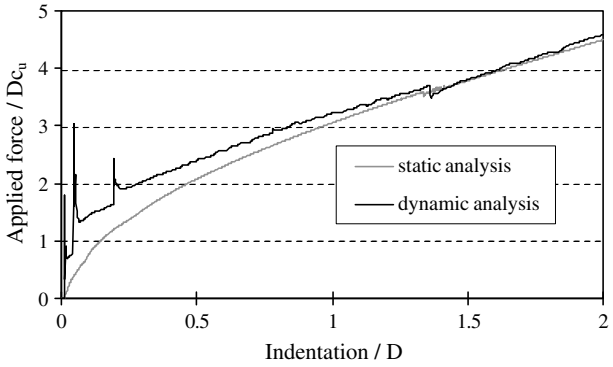

Fig. 7. Load–displacement curves.

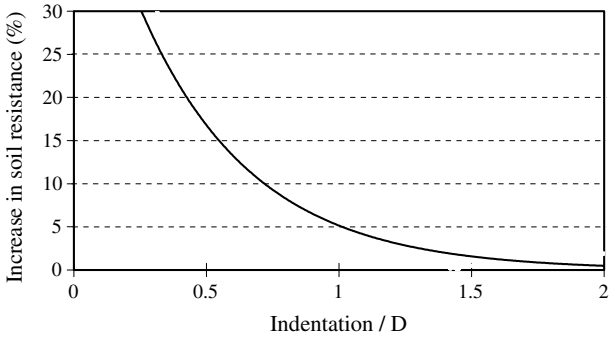

Fig. 8. Increase in soil resistance due to inertia effects.

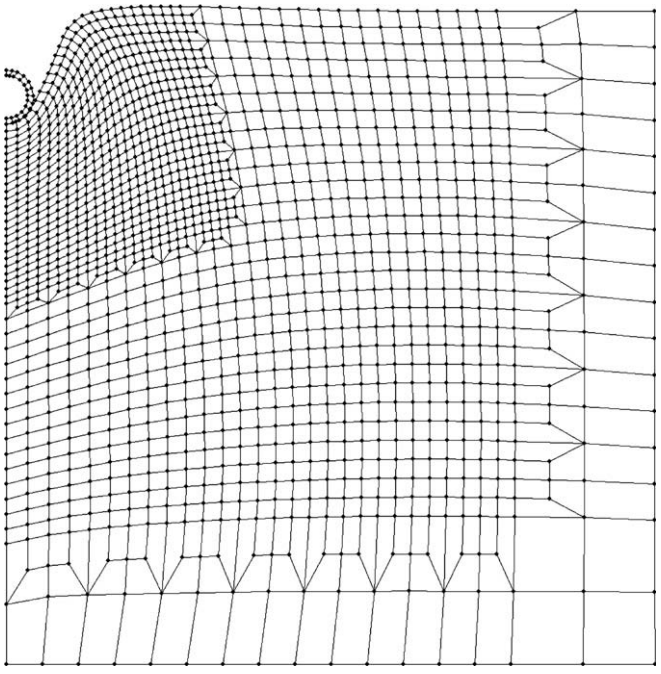

Fig. 9. Deformed mesh at the end of dynamic analysis by the ALE method.

clearly shows the robustness of the proposed ALE method in dynamic analysis of geotechnical problems involving large deformation as well as contact mechanics.

5. Conclusions

An ALE method based on the operator-split technique for solving dynamic geotechnical problems was presented. A spherical cavity under impulse pressure, a layer of soil indented rapidly by a rigid cylinder and a layer of soil loaded dynamically by a footing at various rates were analysed. Some general, but important, conclusions are obtained as follows.

The effect of inertia forces should not be neglected in geotechnical problems involving rapid loading. For the problems considered in this paper, it was shown that the load–displacement response of a rigid footing is generally stiffer under dynamic loading compared to the response predicted by a static analysis. If small deformations are assumed, the predicted collapse load also seems to increase with the rate of loading. Moreover, the limited set of results presented here indicates that the stiffness increases significantly with the rate of applied loading. It would appear that this rate or inertial effect has not previously been investigated in the literature, at least not for an elastoplastic soil. The problem requires more numerical simulations as well as further theoretical investigations in order to be fully understood. This conclusion is valid for both the small deformation and large deformation assumptions.

The main drawback of the UL method is mesh distortion. The ALE method presented here can successfully solve rigid footing and indentation problems involving relatively large deformations as well as dynamic loads. Thus, the ALE method may be applied in solving other important geotechnical problems such as the fast penetration of objects into soil and the dynamic compaction ofsoil. The authors intend to address such problems in future publications.

References

[1] Bayoumi HN, Gadala MS. A complete finite element treatment for the fully coupled implicit ALE formulation. Comput Mech 2004;33:435–52.
[2] Belytschko T, Kennedy JM. Computer models for subassembly simulation. Nucl Eng Des 1978;49:17–38.
[3] Benson DJ. An efficient, accurate and simple ALE method for nonlinear finite element programs. Comput Meth Appl Mech Eng 1989;72:305–50.
[4] Chung J, Hulbert GM. A time integration algorithm for structural dynamics with improved numerical dissipation: the generalized-α method. J Appl Mech 1993;60:371–5.
[5] Gadala MS, Wang J. ALE formulation and its application in solid mechanics. Comput Meth Appl Mech Eng 1998;167:33–55.
[6] Ghosh S, Kikuchi N. An arbitrary Lagrangian–Eulerian finite element method for large deformation analysis of elastic-viscoplastic solids. Comput Meth Appl Mech Eng 1991;86:127–88.
[7] Hirt CW, Amsden AA, Cook JL. An arbitrary Lagrangian–Eulerian computing method for all flow speeds. J Comput Phys 1974;14:227–53.
[8] Hu Y, Randolph MF. A practical numerical approach for large deformation problems in soils. Int J Numer Anal Meth Geomech 1998;22:327–50.
[9] Huetink J, Vreede PT. Progress in mixed Eulerian–Lagrangian finite element simulation of forming processes. Int J Numer Meth Eng 1990;30: 1441–57.
[10] Huerta A, Casadei F. New ALE applications in nonlinear fast-transient solid dynamics. Eng Comput 1994;11:317–45.
[11] Hughes TJR, Liu WK, Zimmermann TK. Lagrangian–Eulerian finite element formulation for incompressible viscous flow. Comput Meth Appl Mech Eng 1981;58:19–36.
[12] Kellezi L. Dynamic soil-structure interaction. Transmitting boundary for transient analysis. PhD Thesis, Series R No. 50, Department of Structural Engineering & Materials, DTU, Denmark; 1998.
[13] Kontoe S, Zdrakovic L, Potts DM. An assessment of time integration schemes for dynamic geotechnical problems. Comput Geotech 2007;35:253–64.
[14] Kontoe S. Development of time integration schemes and advanced boundary conditions for dynamic geotechnical analysis. PhD thesis, Imperial College, University of London, 2006.
[15] Liu WK, Belytschko T, Chang H. An arbitrary Lagrangian–Eulerian finite element method for path-dependant materials. Comput Meth Appl Mech Eng 1986;58:227–45.
[16] Liu WK, Chang H, Chen JS, Belytschko T. Arbitrary Lagrangian–Eulerian Petrov–Galerkin finite elements for nonlinear continua. Comput Meth Appl Mech Eng 1988;68:259–310.
[17] Lysmer JR, Kuhlemeyer L. "Finite dynamic model for infinite media," J Eng Mech Div, ASCE, 95(EM4);859-77.

[18] Nazem M, Sheng D, Carter JP. Stress integration and mesh refinement in numerical solutions to large deformations in geomechanics. Int J Numer Meth Eng 2006;65:1002–27.
[19] Nazem M, Sheng D, Carter JP, Sloan SW. Arbitrary Lagrangian–Eulerian method for large-strain consolidation problems. Int J Numer Anal Meth Geomech 2008;32:1023–50.
[20] Noh WF. A time-dependent two-space-dimensional coupled Eulerian–Lagrangian code. In: Alder B, Fernbach S, Rotenberg M, editors. methods in computational physics, vol. 3. New York: Academic Press; 1964.
[21] Rodriguez-Ferran A, Perez-Foguet A, Huerta A. Arbitrary Lagrangian–Eulerian formulation for hyperelastoplasticity. Int J Numer Meth Eng 2002;53:1831–51.
[22] Sharpe JA. The production of elastic waves by explosion pressures. I. Theory and empirical field observations. Geophysics 1942;7:1–26.
[23] Sloan SW, Abbo AJ, Sheng D. Refined explicit integration of elastoplastic models with error control. Eng Comput 2001;18:121–54.
[24] Sloan SW, Abbo AJ, Sheng D. Erratum. Eng Comput 2002;19:594.
[25] Stein LR, Gentry RA, Hirt CW. Computational simulation of transient blast loading on three-dimensional structures. Comput Meth Appl Mech Eng 1977;11:57–74.
[26] Yamada T, Kikuchi F. An arbitrary Lagrangian–Eulerian finite element method for incompressible hyperelasticity. Comput Meth Appl Mech Eng 1993;102:149–77.